Chemical Geology 275 (2010) 243–253

Contents lists available at ScienceDirect

Chemical Geology

journal homepage: www.elsevier.com/locate/chemgeo

Research paper

In situ sulfur isotope analysis of sulfide minerals by SIMS: Precision and accuracy, with application to thermometry of ~3.5 Ga Pilbara cherts

Reinhard Kozdon [a,*], Noriko T. Kita [a], Jason M. Huberty [a], John H. Fournelle [a], Craig A. Johnson [b], John W. Valley [a]

[a] WiscSIMS and NASA Astrobiology Institute, Department of Geoscience, University of Wisconsin, 1215 W. Dayton St., Madison, WI 53706, USA
[b] U.S. Geological Survey, Denver, CO 80225, USA

ARTICLE INFO

Article history:
Received 20 October 2009
Received in revised form 13 May 2010
Accepted 17 May 2010

Editor: R.L. Rudnick

Keywords:
Sphalerite
Ion microprobe
SIMS
Sulfur isotopes
NBS-123
Crystal orientation effects

ABSTRACT

Secondary ion mass spectrometry (SIMS) measurement of sulfur isotope ratios is a potentially powerful technique for *in situ* studies in many areas of Earth and planetary science. Tests were performed to evaluate the accuracy and precision of sulfur isotope analysis by SIMS in a set of seven well-characterized, isotopically homogeneous natural sulfide standards. The spot-to-spot and grain-to-grain precision for $\delta^{34}S$ is ±0.3‰ for chalcopyrite and pyrrhotite, and ±0.2‰ for pyrite (2SD) using a 1.6 nA primary beam that was focused to 10 μm diameter with a Gaussian-beam density distribution. Likewise, multiple $\delta^{34}S$ measurements within single grains of sphalerite are within ±0.3‰. However, between individual sphalerite grains, $\delta^{34}S$ varies by up to 3.4‰ and the grain-to-grain precision is poor (±1.7‰, $n=20$). Measured values of $\delta^{34}S$ correspond with analysis pit microstructures, ranging from smooth surfaces for grains with high $\delta^{34}S$ values, to pronounced ripples and terraces in analysis pits from grains featuring low $\delta^{34}S$ values. Electron backscatter diffraction (EBSD) shows that individual sphalerite grains are single crystals, whereas crystal orientation varies from grain-to-grain. The 3.4‰ variation in measured $\delta^{34}S$ between individual grains of sphalerite is attributed to changes in instrumental bias caused by different crystal orientations with respect to the incident primary Cs^+ beam. High $\delta^{34}S$ values in sphalerite correlate to when the Cs^+ beam is parallel to the set of directions <*uuw*>, from [111] to [110], which are preferred directions for channeling and focusing in diamond-centered cubic crystals. Crystal orientation effects on instrumental bias were further detected in galena. However, as a result of the perfect cleavage along {100} crushed chips of galena are typically cube-shaped and likely to be preferentially oriented, thus crystal orientation effects on instrumental bias may be obscured. Test were made to improve the analytical precision of $\delta^{34}S$ in sphalerite, and the best results were achieved by either reducing the depth of the analysis pits using a Köhler illuminated primary beam, or by lowering the total impact energy from 20 keV to 13 keV. The resulting grain-to-grain precision in $\delta^{34}S$ improves from ±1.7‰ to better than 0.6‰ (2SD) in both procedures. With careful use of appropriate analytical conditions, the accuracy of SIMS analysis for $\delta^{34}S$ approaches ±0.3‰ (2SD) for chalcopyrite, pyrite and pyrrhotite and ±0.6‰ for sphalerite. Measurements of $\delta^{34}S$ in sub-20 μm grains of pyrite and sphalerite in ~3.5 Ga cherts from the Pilbara craton, Western Australia show that this analytical technique is suitable for *in situ* sulfur isotope thermometry with ±50 °C accuracy in appropriate samples, however, sulfides are not isotopically equilibrated in analyzed samples.

1. Introduction

Since the pioneering work of Thode et al. (1949), sulfur isotope geochemistry has evolved into a powerful tool for investigating igneous, metamorphic, sedimentary, hydrothermal, and biologic processes on Earth (e.g. Seal, 2006). In an early application of *in situ* secondary ion mass spectrometry (SIMS) to sulfur isotopes, Pimminger et al. (1984) used a 10–30 μm diameter beam to analyze $\delta^{34}S$ in galena with a precision of 2–3‰. Since then, SIMS has been increasingly used for the microanalysis of sulfur isotope ratios in sulfides from grain mounts and thin sections, typically with ~15 to 30 μm analysis pits and an analytical precision of 0.5 to 2‰, 2SD (e.g. Eldridge et al., 1987; Graham and Valley, 1992; McKibben and Riciputi, 1998; Fayek, 2009). The analysis of sulfur isotopes by SIMS is facilitated by significant advantages over other stable isotope systems. The $^{34}S/^{32}S$ ratio is ~1/23, allowing more favorable counting statistics than for stable isotope ratios of carbon ($^{13}C/^{12}C$ ~1/89) or oxygen ($^{18}O/^{16}O$ ~1/500). Many sulfide minerals are electrically conductive, enhancing charge neutralization. In addition, sulfur has a high electron affinity, which results in high negative-secondary-ion yields (e.g. Hervig, 2002).

For the best precision and accuracy of *in situ* SIMS analysis, a thorough evaluation of standards for chemical and isotopic homogeneity is required. Further, a mineral- and chemistry-specific instrumental

* Corresponding author. Tel.: +1 608 265 2601; fax: +1 608 262 0693.
E-mail address: rkozdon@geology.wisc.edu (R. Kozdon).

0009-2541/$ – see front matter © 2010 Elsevier B.V. All rights reserved.
doi:10.1016/j.chemgeo.2010.05.015

bias, also called instrumental mass fractionation (IMF), is caused by effects at a variety of stages during SIMS analysis including sputtering, ionization, extraction, transmission and detection of the secondary ions (e.g. Riciputi et al., 1998; Valley and Kita, 2009). The best precision and accuracy are attained if a standard of similar crystal structure and chemical composition is cast in the same mount as the unknown material (Valley et al., 1998; Kita et al., 2009).

In the course of evaluating a new suite of natural sulfide minerals as sulfur isotope standards for SIMS, we analyzed eight different sphalerite samples and were unable to obtain high precision and demonstrate grain-to-grain homogeneity in a suitable standard using a ~10 μm Cs^+ primary beam with Gaussian density distribution around the center of the beam spot ("Gaussian-beam"). In contrast, using the same analytical conditions, we obtained excellent spot-to-spot and grain-to-grain precision of ±0.3‰ (2SD) for chalcopyrite, pyrrhotite, and ±0.2‰ for pyrite. Previous studies have reported difficulties in obtaining a homogeneous sphalerite standard for SIMS. Riciputi et al. (1998) analyzed several sulfide minerals (chalcopyrite, pyrrhotite, and pyrite) with analytical precisions between ±0.4 and ±0.7‰ (2SD), whereas the best precision achieved for sphalerite was ±1.2‰; however, these results were not further discussed. In a subsequent study by Peevler et al. (2003), the reported precision for sphalerite was ±1.6‰ (2SD).

Sputtering is a complex process that results in the formation of secondary ions and molecules, neutral species, electrons, and ion implantation. A variety of physical phenomena are known to form microstructures on sputtered surfaces that have been variously termed steps, terraces, ripples, etch pits, and nano-dots. Ripple production from ion bombardment has been observed for a variety of materials such as Si (e.g. Lewis et al., 1980; Fares et al., 2004); Al, Au, and Cu (Kaminsky, 1965), GaAs, and InP (e.g. Duncan et al., 1983; Malherbe, 2003). Reports of ripple formation in SIMS analysis pits are limited (e.g. Stevie et al., 1988; Fares et al., 2004), and the impact of pit microstructures on the analytical precision of SIMS measurements has not been studied in detail previously. However, the appearance of SIMS analysis pits should be evaluated carefully as important analytical parameters such as erosion rate, ionization yield, and sputter yield are affected. Each of these parameters can cause a significant shift of the instrumental bias (Eiler et al., 1997; Riciputi et al., 1998; Fares et al., 2004) and hence degrade analytical precision.

Until recently, the possibility of isotopic fractionation arising from crystal orientation effects has not been generally considered a problem for SIMS measurements of isotope ratios. One previous SIMS study attributed variation of 10‰ in oxygen isotope ratios to crystal orientation effects in magnetite, but the inconsistency with earlier studies that reported significantly better precision was not addressed (Valley and Graham, 1991; Eiler et al., 1997; Lyon et al., 1998). Huberty et al. (in press) evaluated the effect of crystal orientation on the accuracy of $\delta^{18}O$ analyses in magnetite and hematite by SIMS in detail. It was found that the influence of crystal orientation effects on measured $\delta^{18}O$ in these minerals can be minimized by reducing the total impact energy of the primary ions from 20 to 13 keV and thereby reducing the impact angle from 21° to 14° from normal to the sample surface.

In the first part of this study, we report an analytical protocol to perform high precision (±0.3‰, 2SD, grain-to-grain) *in situ* sulfur isotope measurements by SIMS in a suite of well-characterized, isotopically homogeneous natural sulfide minerals, chalcopyrite, pyrrhotite, and pyrite. In the second part, we address the analytical challenge of high precision and accuracy for *in situ* $\delta^{34}S$ measurements in sphalerite by SIMS. In particular, we evaluate the effect of crystal orientation on instrumental bias and present an analytical protocol to perform measurements of $\delta^{34}S$ in sphalerite with a grain-to-grain precision of ±0.6‰ (2SD). Further, we demonstrate an application of this method and discuss results from *in situ* $\delta^{34}S$ measurements in assemblages of sub-microgram grains of pyrite and sphalerite in ~3.5 Ga cherts from the Trendall Locality and Old Exploration Camp of the North Pole dome, Western Australia.

2. Samples and preparation

A suite of 22 natural sulfide samples including chalcopyrite, galena, pyrrhotite, pyrite, and sphalerite were studied, and seven samples are indicated to be suitable standards for S-isotope measurements by SIMS. The BT-4 and NBS-123 sphalerite, UWPy-1 pyrite, Balmat galena and UWGal-1 galena (Hut, 1987; Crowe et al., 1990; Graham and Valley, 1992; Crowe and Vaughan, 1996) are from the upper amphibolite facies Balmat deposit in the NW Adirondack Lowlands, New York. UWPy-1 pyrite is a new sample of Balmat pyrite previously described by Crowe et al. (1990) and Graham and Valley (1992). The BT-4 sphalerite used for this study is derived from the rock sample 00BT-4, and UWGal-1 galena from the rock sample 89BT-100. Other sphalerite samples from the collections of the Department of Geoscience at UW-Madison, evaluated in this study, were collected at the Universal Exploration Company Mine, located in the Mascot-Jefferson City Zinc District, Tennessee; the Kenoyer Mine in Oklahoma, a Mississippi Valley type deposit, and the Santander Mine in Peru, where zinc–lead mineralization is high temperature carbonate replacement type.

Anderson pyrrhotite (Crowe et al., 1990) selected for SIMS measurements was previously described as a suitable sulfur isotope standards for *in situ* laser microprobe analysis with ~200 μm spatial resolution (Crowe and Vaughan, 1996) and was further used by Mojzsis et al. (2003) for SIMS measurements with ~25 μm spot size. Chisel chalcopyrite was collected from the Chisel Lake deposit in north central Manitoba (Galley et al., 1993; Crowe and Vaughan, 1996). PO-1 pyrrhotite is of unknown origin.

For each sample, 5 to 20 individual 300–500 μm fragments, taken from ~0.5 g crushed chips, were picked and cast with three grains of UWPy-1 pyrite as bracketing standard within 5 mm of the center of a 25 mm epoxy mount. Subsequently, the sample mount was ground to the desired level on a fixed 6 μm diamond mesh pad, followed by 6 μm and 3 μm diamond polishing, and 0.05 μm colloidal silica finishing. After cleaning in deionized water and ethyl alcohol, the epoxy mount was gold coated. This geometry and polishing procedure minimizes instrumental bias related to sample position and polishing relief (Kita et al., 2009). After SIMS measurement, the sample mount was prepared for electron backscatter diffraction (EBSD). SIMS analysis pits were removed by 3 μm diamond polishing and subsequent ~1 h polishing with 0.05 μm colloidal silica on a high-nap pad.

In addition to the standard mounts, petrographic thin sections were prepared from ~3.5 Ga cherts sampled at the Trendall Locality (sample 01MB 39) and Old Exploration Camp (samples 01MB 50 and 01MB 54) from the North Pole dome, Pilbara Craton, Western Australia. The petrographic thin sections were ground into 25 mm rounds, and two 0.75 mm holes were drilled within 5 mm of the center to accommodate grains of UWPy-1 standard. The holes were filled with epoxy and repolished using 6 μm, 3 μm, and 1 μm diamonds.

3. Experimental procedures

3.1. Isotopic composition of the sulfur isotope standards

For UWPy-1 and BT-4 ZnS standards, 100 mg of fragments, that were derived from 0.5 g crushed chips, were sieved in two size fractions (UWPy-1: 50–250 and 250–500 μm, BT-4: <500 and >500 μm). 50 mg of UWGal-1 was in a single size fraction (200–500 μm). The isotopic compositions of the ion microprobe standards were measured at the U.S. Geological Survey in Denver by the continuous flow method using a Costech elemental analyzer coupled to a Thermo Finnigan Delta Plus XP mass spectrometer (Table 1). Aliquots corresponding to about 50 μg of sulfur were weighed into tin capsules with vanadium pentoxide powder and then loaded into the autosampler along with similarly prepared aliquots of IAEA-S-1 and S-2 calibration standards. The analytical procedure was a slight modification of the method of Giesemann et

al. (1994). Delta values are reported relative to VCDT on a scale where IAEA-S-1 and IAEA-S-2 are assigned values of −0.3 and 22.67‰, respectively (Ding et al., 2001). Aliquots of the NBS-123 sphalerite standard that were analyzed along with the unknowns gave 18.13 ± 0.12‰ ($n = 8$).

3.2. Electron microprobe analysis

Electron microprobe analysis (EPMA) of the sulfide samples (Table 2 and supplementary material, Table 2) was performed with a CAMECA SX51 at UW-Madison, operated at 20 kV, a Faraday cup current of 30 nA and a focused beam. Four to six individual grains of Chisel chalcopyrite, Balmat Galena, UWPy-1, Anderson pyrrhotite, PO-1 pyrrhotite and BT-4 sphalerite were analyzed at 3 to 10 spots each. The Pb Mα line was used, and Pb on Cd Lα interference was corrected. Differential mode pulse height analysis (PHA) was utilized for possible higher order interferences on Fe, Ni, Cu and Zn. The standards were troilite for Fe, galena for Pb, and standards synthesized by G. Czamanske for Cu ($CuFeS_2$), Zn (ZnS), Ni (NiS_2), Cd (CdS), Hg (HgTe), and Mn (MnS). Sulfur Kα was used from the specific sulfide standard comparable to the sulfide unknown. Care was taken to verify the S Kα peak position for each sulfide type due to its known chemical shift. Peak and background counting times were 10 s each. The matrix correction algorithm utilized was Armstrong/Love Scott (Armstrong, 1988).

3.3. SIMS analysis of $\delta^{34}S$

In situ sulfur isotope analysis ($^{34}S/^{32}S$) by SIMS was performed at the WiscSIMS Laboratory, UW-Madison, using a CAMECA IMS-1280 high resolution, multi-collector ion microprobe. The instrumental conditions are similar to those described for oxygen two-isotope analysis with nearly full secondary ion transmission (Kita et al., 2009). Although most sulfide minerals are either conductors or semiconductors, the sulfide grain mounts in epoxy resin were Au-coated (~50 nm), and the electron gun was used for surface charge compensation. An energy window of 40 eV was set at the low energy band. The secondary $^{34}S^-$ and $^{32}S^-$ ions were simultaneously collected by two Faraday cup detectors. Mass resolving power (MRP, $M/\Delta M$), measured at 10% peak height, was set to 2200. Zn^{2-} interferences were not detected. After UWPy-1 was found to be homogeneous by SIMS, it was used as bracketing standard to monitor instrument stability and the analytical spot-to-spot reproducibility. Grains of UWPy-1 were cast in the center of each sample mount and were measured in at least four spots before and after every 10 to 20 sample analyses. The precision of a set of bracketing UWPy-1 analyses is on average equal to ±0.20‰ (2SD). Raw measured $^{34}S/^{32}S$ ratios were converted to the delta notation $\delta^{34}S$ by normalizing to Vienna Cañon Diablo Troilite $(^{34}S/^{32}S)_{VCDT} = 0.044163$ (Ding et al., 2001).

Three different analytical modes were applied to evaluate the effect of crystal orientation on instrumental bias.

3.3.1. Deep-pit mode

In the routine analytical condition, a primary $^{133}Cs^+$ beam with an intensity of ~1.6 nA was focused to 10 μm diameter with a Gaussian density distribution. The primary and secondary ion accelerating voltages were +10 kV and −10 kV, so that the total impact energy of the primary ions is 20 keV. This condition is aimed to obtain secondary $^{32}S^-$ ion intensities higher than 10^9 cps and is similar to that of oxygen isotope analysis of silicates, oxides, and carbonates (Kita et al., 2009). The dish-shaped SIMS analysis pits formed by the Gaussian focused beam have a depth of 4 to 6 μm. This analytical approach is referred to as "deep-pit mode". Chalcopyrite, galena, pyrrhotite, pyrite and sphalerite were analyzed in deep-pit mode. The secondary $^{32}S^-$ ion intensity varied from ~1.5×10^9 cps for pyrrhotite to ~2.6×10^9 cps for sphalerite. The total analytical time was about three minutes per pit: 10 s presputtering; ~1 min automatic centering of the secondary ions in the field aperture, and a total of 80 s integration of secondary ions (20 cycles of 4 s each). It is important to note that sulfur isotope ratios change systematically during the analysis, so that the spot-to-spot reproducibility on a homogeneous sample is often better then the internal precision (see Kita et al., 2009; Valley and Kita, 2009). Thus, in order to achieve the highest precision, consistent analytical conditions (stable primary beam and carefully timed analysis routine) are essential.

3.3.2. Shallow-pit mode

As an experiment, the routine analytical condition was modified by using a ~20 μm oval-shaped Köhler illuminated primary beam of $^{133}Cs^+$ with a low ion intensity of ~0.3 nA. SIMS analysis pits created by a Köhler illuminated beam are 0.15 μm deep, and this analytical method is referred to as "shallow-pit mode". Measurements were performed for BT-4 sphalerite and UWPy-1 on the same set of grains that were previously analyzed in deep-pit mode. The secondary $^{32}S^-$ ion intensity was 2.3×10^8 cps for pyrite and 4.7×10^8 cps for sphalerite. In order to further minimize the depth of the analysis pits, the total presputtering time was set to 100 s (including ~60 s automated centering of the secondary ions in the field aperture), so that the integration of secondary ions (first analytical cycle) started as soon as the secondary ion yield approached ~70% of its plateau. The total integration time was 40 s (20 cycles of 2 s each), and the total analytical time per pit about 2.5 min. Additional analyses were made adjacent to some of the previous pits for a total integration time of 120 s (60 cycles) to evaluate the effect of increasing sputtering depth on the measured isotope ratios.

Further, measurements were made in two individual sphalerite grains using a small energy offset to investigate the effect of energy-dependent instrumental bias on variation in measured $\delta^{34}S$ (e.g. Hervig et al., 1992; Eiler et al., 1997; Hervig, 2002). The threshold of the energy window of 40 eV was raised by +10 eV (10 to 50 eV). At this setting, the secondary ion yield on $^{32}S^-$ was cut by 50% from ~4.7×10^8 cps to ~2.5×10^8 cps; a larger energy offset would have reduced the secondary ion yield below the limit for high precision Faraday cup collection mode.

3.3.3. Reduced total impact energy

The routine analytical condition was further modified by reducing the total impact energy from 20 keV (+10 kV primary and −10 kV secondary accelerating voltage) to 13 keV (+3 kV primary and −10 kV secondary accelerating voltage). As a result of the voltage settings, the $^{133}Cs^+$ primary ion beam spot was elongated with a size of ~12×20 μm. In the first analytical session, a ~0.3 nA Köhler illuminated primary beam was used, however, the resulting pits were dished-shaped. In the second session, a ~0.4 nA Gaussian beam was used. The SIMS analysis pits had a final depth of ~0.5 μm. Analyses at a total impact energy of 13 keV were performed in the same grains that were previously analyzed in deep-pit and shallow-pit modes. Typically, the secondary $^{32}S^-$ ion intensity was 6.5×10^8 cps for pyrite and 7.5×10^8 cps for sphalerite. The total analysis time per pit was about 4 min: 60 s presputtering; ~1 min automatic centering of the secondary ions in the field aperture, and a total of 80 s integration of secondary ions (20 cycles of 4 s each). In order to evaluate crystal

Table 1
Calibration of S-isotope standards by gas-source mass spectrometer.

Sample #	n	$\delta^{34}S$ (‰ VCDT)[a]
BT-4<500 μm	3	15.42 ± 0.07
BT-4>500 μm	5	15.23 ± 0.09
UWPy-1 50–250 μm	3	16.30 ± 0.19
UWPy-1 250–500 μm	4	16.39 ± 0.20
UWGal-1 200–500 μm	4	16.61 ± 0.08
NBS-123	8	18.14 ± 0.13

[a] VCDT scale after Ding et al. (2001). Precision quoted at 1SD.

Table 2
Electron microprobe analyses of sulfides.

	n grains	*n* meas.	Cd wt.%	Hg wt.%	S wt.%	Mn wt.%	Fe wt.%	Ni wt.%	Cu wt.%	Zn wt.%	Pb wt.%	Totals
UWPy-1												
Average ± 1 SD	5	15	n.d.	n.d.	53.01 0.32	n.d.	46.76 0.18	n.d.	n.d.	n.d.	n.d.	99.77
Balmat sphalerite BT-4												
Average ± 1 SD	5	25	0.15 0.02	n.d.	33.00 0.06	0.09 0.03	5.09 0.11	n.d.	n.d.	62.26 0.18	n.d.	100.50
Kenoyer sphalerite												
Average ± 1 SD	5	25	0.47 0.14	n.d.	33.06 0.06	n.d.	n.d.	n.d.	n.d.	66.48 0.36		100.20
Anderson pyrrhotite												
Average ± 1 SD	4	16	n.d.	n.d.	39.40 0.25	n.d.	60.23 0.33	n.d.	n.d.	n.d.	n.d.	99.63
PO-1 pyrrhotite												
Average ± 1 SD	6	18	n.d.	n.d.	39.07 0.18	n.d.	61.06 0.17	n.d.	n.d.	n.d.	n.d.	100.13
Chisel chalcopyrite												
Average ± 1 SD	4	37	n.d.	n.d.	34.52 0.06	n.d.	30.58 0.07	n.d.	34.29 0.31	n.d.	n.d.	99.39
Balmat galena												
Average ± 1 SD	4	22	n.d.	n.d.	13.47 0.06	n.d.	n.d.	n.d.	n.d.	n.d.	86.49 0.66	99.96

n.d. = below detection limit.

orientation effects on instrumental bias, grains of BT-4 sphalerite were analyzed with the sample mount rotated 90° from the previous placement in the SIMS sample holder.

3.4. EBSD analysis

EBSD measurements were performed to determine the crystal orientation of individual sphalerite grains using a Hitachi S-3400N Scanning Electron Microscope (SEM) with an accelerating voltage of 20 kV. The Electron Backscatter Patterns (EBSPs) were collected on a phosphor screen, digitized, and processed by the software package CHANNEL5 (Oxford Instruments, Ltd.). EBSD data were acquired in point collection mode, and one to five EBSPs were taken for each grain with a mean angular deviation (MAD) of less than 1°. The EBSP with the lowest MAD for each individual grain was selected and plotted on a lower-hemisphere equal area projection using the software Stereo32, Version 1.01 (Röller and Trepmann, 2008). The incident angle (θ) of the SIMS primary Cs^+ beam, from normal to the sample surface, is a function of the primary axis angle (α) and the primary (V_p) and secondary (V_s) accelerating voltages, and was calculated using the following equation (CAMECA, 2004):

$$\sin\theta = \frac{\sin(\alpha = 30^\circ)}{\sqrt{1 - V_s / V_p}}$$

For primary and secondary accelerating voltages of + 10 kV and − 10 kV respectively, the incident Cs^+ beam angle is 20.7° from normal to the sample surface, and 14° for analyzes with a reduced total impact energy of 13 keV. The stereographic projection of the Cs^+ beam direction for each grain was replotted in a common reference frame within the cubic standard triangle (defined as the area between the [111], [110], and [100] directions) on a [111]-centered stereographic projection (Huberty et al., in press). Uncorrected values of measured $\delta^{34}S(Sphal)_{Raw}$ were assigned to the Cs^+ beam directions for individual grains, and the stereographic projection was contoured for $\delta^{34}S(Sphal)_{Raw}$ using block kriging and radial basis function gridding methods with the software package 3DFieldPro (Galouchko, 2008).

4. Results

4.1. Deep-pit mode

Results of the SIMS sulfur isotope analyses are summarized in Table 3. A precision of ± 0.3‰ or better (2SD) was obtained for $\delta^{34}S$ measurements on multiple grains of Chisel chalcopyrite (± 0.26‰, $n = 20$), Anderson pyrrhotite (± 0.32‰, $n = 8$), PO-1 pyrrhotite (± 0.27‰, $n = 8$), and UWPy-1 (± 0.20‰, $n = 92$). Similarly, multiple $\delta^{34}S$ measurements have a precision of ± 0.3‰ within single grains of sphalerite (Fig. 1). In contrast, after testing eight potential sphalerite standards for *in situ* SIMS, the best grain-to-grain precision obtained was ± 1.7‰ (2SD, $n = 20$) for sphalerite BT-4 (Fig. 2). The range in measured $\delta^{34}S$ between individual grains of BT-4 sphalerite is 3.4‰ and $\delta^{34}S$ correlates well ($R^2 = 0.87$, $n = 20$, Fig. 3) with secondary ion yield, defined as the ratio of the number of secondary ions detected and the primary beam intensity. The secondary ion yield varies by 18%, from ~ 2×10^9 cps/nA for analyses with high $\delta^{34}S(Sphal)_{Raw}$ values to ~ 2.3×10^9 cps/nA for grains with low $\delta^{34}S(Sphal)_{Raw}$ values (Supplementary material, Tables 3 and 7).

The depth of the SIMS analysis pits in sphalerite varies from 4 to 6 µm as determined by a ZYGO™ white light profilometer (Fig. 4A–C). Both the secondary ion yield and measured $\delta^{34}S(Sphal)_{Raw}$ values are grain specific and can be duplicated by repeated analysis of the same grain (Fig. 1). Thus, if only a single grain of sphalerite is measured by SIMS, the analyses of samples can be highly reproducible, but not accurate.

Secondary ion yield and measured $\delta^{34}S$ in sphalerite correlate with pit microstructures. Analysis pits with a smooth inner surface are characteristic for low secondary ion yields and high $\delta^{34}S(Sphal)_{Raw}$ values, whereas analysis pits featuring pronounced ripples and terraces are associated with high secondary ion yields and low $\delta^{34}S(Sphal)_{Raw}$ values (Fig. 4A–C and Supplementary data, Table 3). In contrast, SIMS analysis pits in chalcopyrite, galena, pyrite, and pyrrhotite are smooth and do not vary in appearance, and the total range in secondary ion yield varies by 1–3% for each mineral except galena (~ 10%).

Fig. 5 shows the measured $\delta^{34}S(Sphal)_{Raw}$ values and $^{32}S^-$ count rates for each of the 20 cycles in two grains of BT-4 sphalerite

Table 3
In situ δ^{34}S measurements of sulfide samples by SIMS.

Mineral	*n*	Number of grains	^{32}S (cps) $\times 10^9$ average	$\delta^{34}S_{Raw}$ average	2SD	Bias	δ^{34}S ‰VCDT	Reference
S-isotope measurements by ~1.6 nA (1.4 nA in Sessions I+II), deep-pit mode								
Chisel chalcopyrite	16	4	1.9[a]	0.14	0.26			
Trout Lake chalcopyrite	10	5	2.0[a]	−1.41	0.35	−1.7	0.3	Crowe and Vaughan (1996)
Anderson pyrrhotite	8	4	1.5[a]	−2.94	0.32	−4.3	1.4	Crowe and Vaughan (1996)
UWPy-1 [b]	165	10	1.7[a]	17.40	0.17	1.0	16.4	This study
PO-1 Pyrrhotite	8	4	1.2[a]	−1.11	0.27			
Balmat Galena [c]	12	4	2.5	−11.94	0.31			
UWGal-1 [d]	10	5	1.6[a]	−13.03	0.76	−29.6	16.6	This study
Kenoyer Sphalerite	15	15	3.8	−6.76	1.84			
BT-4 Sphalerite	20	20	3.5	12.10	1.71	−3.2	15.3	This study
S-isotope measurements by ~0.3 nA, shallow-pit mode (2nd run)								
BT-4 sphalerite	20	20	0.5	12.53	0.56	−2.8	15.3	This study
S-isotope measurements by reduced primary ions impact energy of 13 keV								
BT-4 sphalerite	41	20	0.5	17.09	0.58	1.8	15.3	This study

[a] Lower count rate due to different beam settings (1.4 nA vs. 1.6 nA in all other sessions).
[b] Combined data from several analytical sessions using deep-pit condition. The average precision of UWPy-1 as a bracketing standard for all measurements performed in this study is 0.20‰ (2SD).
[c] 1st mount, grains were oriented with [100] parallel to normal.
[d] 2nd mount, grains were randomly oriented.

comprising one analysis. Measured δ^{34}S values are plotted for each cycle for grain 9 (low $\delta^{34}S(Sphal)_{Raw}$, high secondary ion yield) and grain 19 (high $\delta^{34}S(Sphal)_{Raw}$, low secondary ion yield). In both grains, the secondary ion yield increases linearly as a function of sputtering time and depth. The difference in secondary ion yield between these two grains is associated with an offset in measured δ^{34}S values of 2.4‰ that remains constant for the course of 20 cycles. These results suggest that the analytical precision cannot be improved by modifications of the analysis time.

4.2. Shallow-pit mode

The grain-to-grain precision of δ^{34}S for BT-4 sphalerite improves significantly from ±1.7‰ in deep-pit mode to ±0.6‰ in shallow-pit mode (2SD, $n=20$, Fig. 6). This gain in analytical precision is accompanied by a smaller variation in the range of secondary ion yield of 9% for analyses made in shallow-pit mode compared to 18% in deep-pit mode (Supplementary data, Tables 3 and 7). Further, there is no correlation between secondary ion yield and measured δ^{34}S (Fig. 3), and the formation of pit microstructures is suppressed (Fig. 4D). The final depth of the SIMS analysis pits is 0.1–0.15 µm in shallow-pit mode, 40 times shallower than pits created in deep-pit mode, which entails 20 times higher primary-beam current density ($\sim 2\times10^{-2}$ nA/µm^2) and twice the analysis time.

In Fig. 7A, the change of measured $\delta^{34}S(Sphal)_{Raw}$ values over the course of 60 analytical cycles of 2 s integration time each is shown for BT-4 sphalerite grain 9 (low $\delta^{34}S(Sphal)_{Raw}$, high ion yield) and grain 19 (high $\delta^{34}S(Sphal)_{Raw}$, low ion yield; compare with Fig. 5 for deep-pit analysis). The difference in measured δ^{34}S ($\Delta^{34}S = \delta^{34}S_{(grain\ 19)} - \delta^{34}S_{(grain\ 9)}$) between these two sphalerite grains, plotted for 60 analytical cycles, is shown in Fig. 7B. Measured $\delta^{34}S(Sphal)_{Raw}$ values from the first 5 cycles are within ~0.5‰ and diverge with increasing sputtering time and depth. Thus, good grain-to-grain precision is only achieved by an early start of the analytical cycles, i.e. ion counting in the Faraday collectors (Fig. 7A,B). For the analytical conditions used in this study, good results were obtained by starting the first analytical cycle when the secondary ion yield approaches about 70% of its plateau (Fig. 7C). This time was carefully evaluated by a presputtering test and was found to be ~110 s. Fig. 7B shows that the grain-to-grain

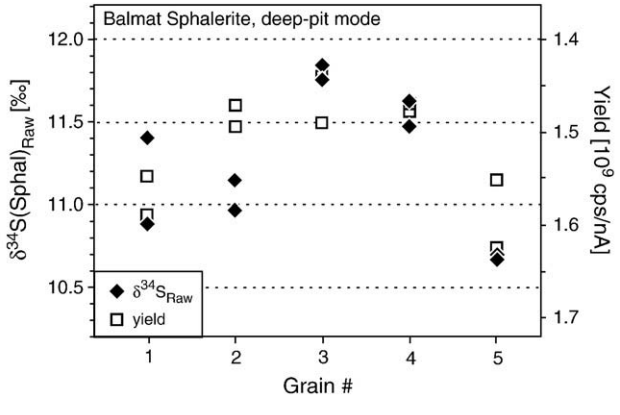

Fig. 1. Values of δ^{34}S and secondary ion yield (^{32}S) for multiple ion microprobe measurements within single grains of Balmat sphalerite (aliquot from the sphalerite described by Crowe et al., 1990) in deep-pit mode. The precision of individual δ^{34}S measurements (black diamonds) is ±0.3‰ (2SD) except for grain #1, but the grain-to-grain precision is worse. Thus, if only a single grain of sphalerite is analyzed by SIMS, the analyses of samples would seem precise, but could be significantly less accurate. The secondary ion yield (white boxes) is inversely correlated (note that right axis scale is reversed). High $\delta^{34}S_{Raw}$ values correspond to grains featuring low secondary ion yields.

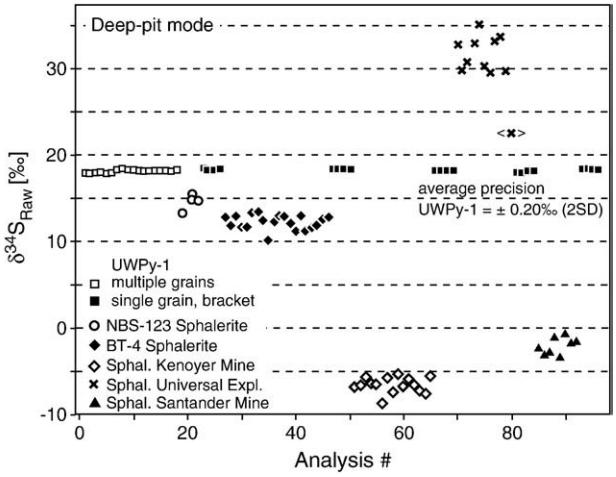

Fig. 2. Measured $\delta^{34}S_{Raw}$ values of UWPy-1 pyrite and individual grains of sphalerite from five different samples analyzed in deep-pit mode. White and black squares show that δ^{34}S analyses in multiple grains of UWPy-1 have the same precision (0.2‰) as within single grains. In contrast, individual δ^{34}S measurements in sphalerite are each from different grains and show considerably more variability than analyses of the bracketing pyrite analyses or of multiple analyses on single crystals of sphalerite (Fig. 1).

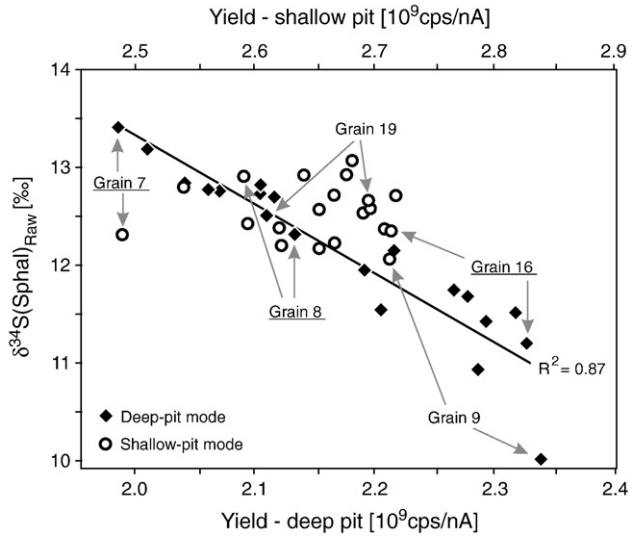

Fig. 3. Values of $\delta^{34}S(Sphal)_{Raw}$ plotted vs. secondary ion yield for twenty grains of BT-4 sphalerite. In deep-pit mode (solid diamonds), the grain-to-grain precision is ±1.7‰ (2SD) and $\delta^{34}S$ correlates with secondary ion yield ($R^2 = 0.87$). In shallow-pit mode (open circles), the grain-to-grain precision for sphalerite is improved to ±0.6‰ (2SD).

precision deteriorates with increasing integration time. The best grain-to-grain precision of ±0.7‰ (1st run) and 0.6‰ (2nd run, 2SD) was obtained by integrating only the first ten of 20 analytical cycles (20 s total integration time, indicated as grey bars in Fig. 7A–C).

4.3. Reduced total impact energy

The same set of 20 grains of BT-4 sphalerite that were used for measurements in shallow- and deep-pit mode was analyzed with a reduced primary accelerating voltage of +3 kV while leaving the secondary accelerating voltage unchanged at −10 kV, so that the total impact energy is 13 keV. The final depth of the dish-shaped SIMS analysis pits formed by Gaussian focused beam is 0.5 µm. The grain-to-grain precision for analyses made at 13 keV is ±0.6‰ (2SD) in Session I, identical to that obtained in shallow-pit mode, and ±0.8‰ in Session II (Supplementary data, Table 4). Thus, the analytical precision of $\delta^{34}S$ measurements in sphalerite is improved by either reducing the depth of the analysis pits using a Köhler illuminated primary beam (shallow pit mode), or by lowering the total impact energy from 20 keV to 13 keV and hereby reducing the incident primary beam angle from 20.7° to 14°.

4.4. Effect of energy offset

In previous studies, it was demonstrated that the analytical precision of *in situ* stable isotope measurements by SIMS can be significantly improved by the application of a high energy offset (Hervig et al., 1992; Riciputi and Paterson, 1994; Valley and Graham, 1996; Eiler et al., 1997). However, these studies employed single-collector instruments with an EM detector and different analytical protocols, and the best spot-to-spot precision was generally in the 1 to 2‰ range. The grain-to-grain precision and potential crystal orientation effects were not strictly evaluated in these studies.

The effect of a higher energy offset on orientation effects in sphalerite was evaluated in the present study under conditions where multiple Faraday cup detectors produce a spot-to-spot reproducibility of 0.3‰. However, increasing energy offset reduces secondary ion yield. In combination with the low-intensity Köhler illuminated beam, the count rate for $^{34}S^-$ at high energy offset is below the limits for high precision imposed by the background of Faraday cup detectors. Thus, the 40 eV energy window was raised by only 10 eV (10 to 50 eV), causing an acceptable reduction in secondary ion yield of 50%. Aside from a small shift in instrumental bias of 0.5‰, the difference in measured $\delta^{34}S$ between two individual grains of BT-4 sphalerite (grain 9, high yield, low $\delta^{34}S_{Raw}$, and grain 19, low yield, high $\delta^{34}S_{Raw}$) remained unchanged (Fig. 7A). Thus, the application of a small energy offset does not reduce the orientation effects found for sphalerite under the analytical conditions used in this study.

4.5. Correlation between $\delta^{34}S$ and crystal orientation

In Fig. 8, the stereographic projection of the Cs^+ beam direction is shown for 20 grains of BT-4 sphalerite and 15 grains of Kenoyer sphalerite (deep-pit mode, Table 2 and Supplementary data, Tables 6 and 7). Sphalerite has −43 m (diamond-centered cubic) point symmetry. Because of the high symmetry in minerals with cubic crystal structures, the lower hemisphere stereographic projection can be divided into 24 standard triangles with corners at the sets of directions <100>, <111>, and <110>. All grains are thus plotted within a single standard triangle conscribed by the corners at [100], [111] and [110] (Fig. 8A,B). EBSD analyses show that the individual grains of sphalerite analyzed in this study are single crystals and that crystal orientation varies from grain-to-grain. In Fig. 8A and B, the stereographic projection of the Cs^+ beam direction for each sphalerite grain is contoured according to the measured $\delta^{34}S(Sphal)_{Raw}$ value at 0.5‰ isopleths. In order to plot BT-4 sphalerite and Kenoyer sphalerite in the same figure, $\delta^{34}S(Sphal)_{Raw}$ values of Kenoyer Sphalerite were adjusted to the same range in $\delta^{34}S$ by the addition of 18.7‰, which is the average difference in raw $\delta^{34}S$ values between these two sphalerite samples.

The highest $\delta^{34}S$ values in sphalerite are shown by light shades of grey ($\delta^{34}S_{Raw} > 11.5$‰) in Fig. 8B. These values correlate with the lowest secondary ion yield and are measured when the Cs^+ beam is parallel to the planar set of directions <*uuw*>, from [111] to [110], which are preferred for channeling and focusing in diamond-centered cubic crystals (Gnaser, 2007).

In Fig. 9, measured values of $\delta^{34}S_{Raw}$ are shown for twenty BT-4 sphalerite grains that were analyzed with the sample mount at two different orientations and at a total impact energy of 13 keV. These grains were analyzed first with the sample mount oriented similar to previous analyses made in deep-pit and shallow-pit modes. Subsequently, the sample mount was rotated by 90°, and the same 20 grains were reanalyzed. In comparison to Fig. 6 where multiple measurements of $\delta^{34}S$ within single grains of BT-4 sphalerite show a maximum difference of 0.14‰, values of $\delta^{34}S$ measured in the same grain before and after rotation of the sample mount vary by up to 0.8‰. The $\delta^{34}S$ values of UWPy-1 pyrite used as bracketing standard show a max. range of 0.2‰ for both orientations of the sample mount (Fig. 9). Thus, the analytical precision obtained in sphalerite is the cumulative effect of the instrumental variability for measurements of a homogeneous standard (spot-to-spot precision of ±0.2‰ for pyrite), and the crystal orientation effects on instrumental bias. As a practical matter, the orientation effect can be evaluated as less than the best measured reproducibility for randomly oriented grains of a standard.

4.6. Orientation effect on bias in galena

Crystal orientation effects on measured values of $\delta^{34}S$ by SIMS were also evaluated in galena. As a result of the perfect cleavage along {100}, crushed chips of galena have the potential to be mounted with a preferred orientation. Thus, crystal orientation effects on the grain-to-grain precision can be masked and are likely to be overlooked. Initially, individual grains of Balmat Galena BT-100 were inadvertently oriented with [100] normal to the polished face, resulting in good grain-to-grain precision of 0.3‰ (2SD, $n = 12$, Fig. 10) and thus erroneously implying the absence of an orientation effect. However, in a second sample mount with randomly oriented grains of Balmat galena (verified by EBSD), the grain-to-grain precision was ±0.76‰

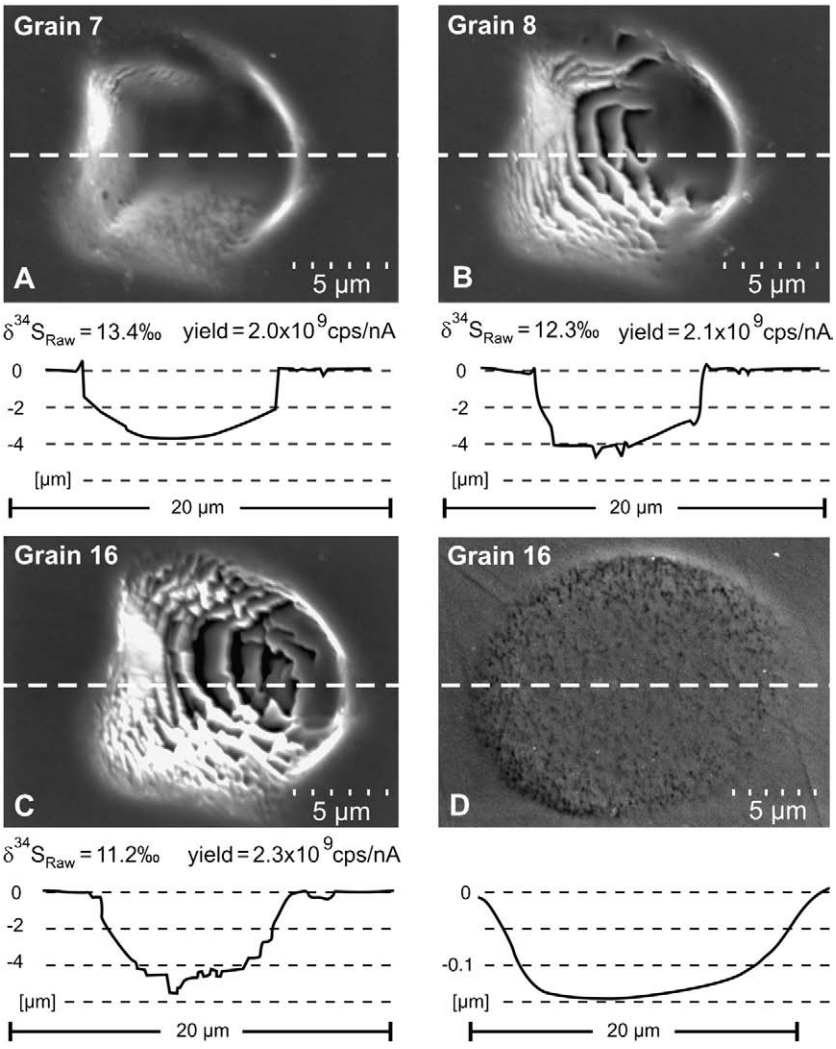

Fig. 4. A–C) The appearance of SIMS analysis pits is shown for BT-4 sphalerite analyses made in deep pit mode. Dashed horizontal lines mark the positions of surface profiles measured by white light profilometer. Different grains of sphalerite are shown with: (A) high ($\delta^{34}S(Sphal)_{Raw} = 13.4‰$, grain 7), (B) medium ($\delta^{34}S(Sphal)_{Raw} = 12.3‰$, grain 8), and (C) low ($\delta^{34}S(Sphal)_{Raw} = 11.2‰$, grain 16) measured $\delta^{34}S$ values. Sulfur isotope ratios are inversely correlated with secondary ion yield. The grains are labeled in Fig. 3. Note the increasing pit depth associated with ripple texture. (D) The formation of surface topography is suppressed by the combination of a Köhler illuminated beam with a short analysis time and low primary beam intensity. Pits formed in shallow-pit mode are 40 times shallower than pits made in deep-pit mode. Images (C) and (D) are from the same grain.

(2SD, $n = 10$) in deep-pit mode. Thus an orientation effect is verified for galena.

4.7. $\delta^{34}S$ of pyrite–sphalerite pairs in ~3.5 Ga cherts, Pilbara Craton

The temperatures of formation of ~3.5 Ga cherts from the Pilbara Craton, Western Australia are of great interest because of controversy surrounding the existence of the oldest recognized microfossils on Earth. Values of $\delta^{34}S$ in pyrite and coexisting sphalerite have potential to record temperatures of deposition, however these sulfide grains show complex textures and individual grains are too small for conventional techniques of bulk analysis. The capabilities of an ion microprobe to perform high precision *in situ* sulfur isotope measurements are ideal for such a study.

The Pilbara cherts are the oldest Archean examples known without significant alteration or high temperature metamorphism. The Pilbara cherts contain putative microfossils (Schopf et al., 2002), however, the interpretations for Archean cellular life are disputed (e.g. Brasier et al., 2006). Evaluating the formation temperature of these samples by means of sulfur isotope thermometry by SIMS has the potential to address ongoing debates about the existence of Archean life. Sulfur isotope thermometry is based on the partitioning of sulfur isotopes

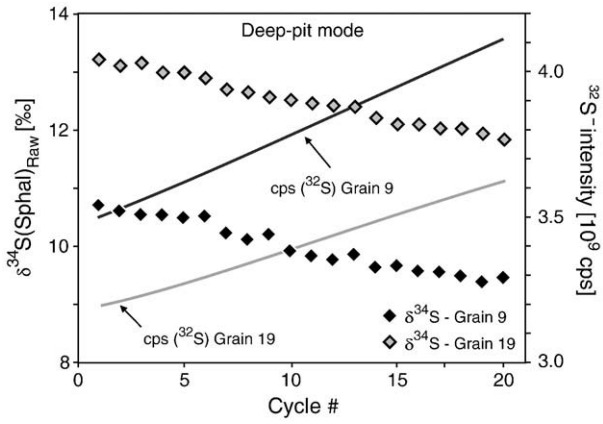

Fig. 5. Values of $\delta^{34}S(Sphal)_{Raw}$ are plotted vs. secondary ion yield for 20 four-second cycles comprising one analysis in deep-pit mode on each of two grains of BT-4 sphalerite. Grain 9 (low $\delta^{34}S(Sphal)_{Raw}$, high ion yield and rippled pit) and grain 19 (high $\delta^{34}S(Sphal)_{Raw}$, low ion yield and smooth analysis pit) are plotted for comparison. A presputtering time of 10 s and centering of the secondary ion image (~60 s) precedes the first analysis cycle. The difference in measured $\delta^{34}S$ between grains 9 and 19 remains constant at ~2.4‰ over the course of the total analysis time.

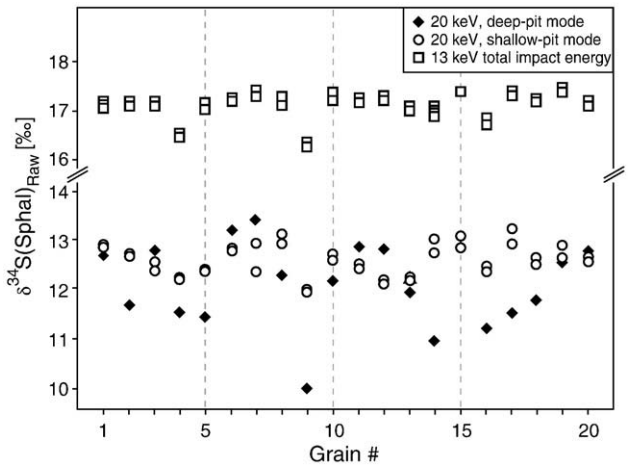

Fig. 6. Comparison of $\delta^{34}S(Sphal)_{Raw}$ values in 20 randomly oriented grains of BT-4 sphalerite using three different analytical modes: (I) black diamonds indicate measurements performed in deep-pit mode, 20 keV, (II) white circles show analyses in shallow-pit mode, 20 keV, and (III) white squares show analyses at 13 keV total impact energy. The grain-to-grain precision improved from ±1.7‰ (2SD) in deep-pit mode to ±0.6‰ in shallow-pit mode and at 13 keV. The ~4‰ shift of $\delta^{34}S(Sphal)_{Raw}$ values between analyses at 20 keV and 13 keV is caused by a change in instrumental mass bias as a result of the different analytical conditions.

between two mineral phases such as pyrite and sphalerite (Kajiwara and Krouse, 1971) and is based on the assumption that the minerals formed contemporaneously in equilibrium with one another. Fig. 11 shows the $\delta^{34}S$ values of coexisting pyrite and sphalerite, measured with a reduced total impact energy of 13 keV in 15–70 μm-diameter grains in ~3.5 Ga cherts sampled at the Old Exploration Camp (01MB 54 and 01MB 50) and the Trendall Locality (01MB 39) in the North Pole dome, Pilbara (Supplementary data, Table 5).

Several grains in all samples are zoned, and measured $\delta^{34}S$ varies by up to 2‰ in adjacent analysis pits. Further, the $\delta^{34}S$ of individual pyrite grains in sample 01MB 39 varies by ~8‰ over a distance of less than 10 mm. The smallest variation in measured $\delta^{34}S$ was found in sample 01MB 54. Still, the grain-to-grain precision of ±2.0‰ for sphalerite and ±0.83‰ (2SD) for pyrite measured in sample 01MB 54 is by a factor of about three worse than the grain-to-grain precision obtained in the standards (±0.2‰ for UWPy-1, ±0.8‰ for BT-4 sphalerite), indicating sample heterogeneity. The average Δ(pyrite–sphalerite) value of 4.6‰ in sample 01MB 54 is outside the range of equilibrium (Kajiwara and Krouse, 1971). For comparison, Δ(pyrite–sphalerite) values between 3.5 and 2.1‰ correspond to formation temperatures of ~20 to 100 °C. Thus, the sulfides in these cherts do not represent isotope equilibrium and are unsuitable for sulfur isotope thermometry. Nevertheless, recognition of this variability is important, as the zonation found in individual grains as well as the variation in measured $\delta^{34}S$ between single grains of pyrite and sphalerite would be masked and obscured by conventional analytical approaches using larger sample weights and/or multiple grains. For instance, the average Δ(pyrite–sphalerite) value of 1.5‰ in sample 01MB 50 could be erroneously interpreted to reflect depositional temperatures of ~150 to 200 °C.

5. Discussion

5.1. Crystal orientation effects and S-MIF

Farquhar et al. (2000) reported the occurrence of sedimentary sulfide and sulfate minerals in Archean rocks, in which the sulfur isotopes do not lie on a mass-dependent fractionation line. The discovery of this signal in geologic materials has potentially important implications for understanding the chemical evolution of the early atmosphere. This so-called mass-independent fractionation (MIF) is

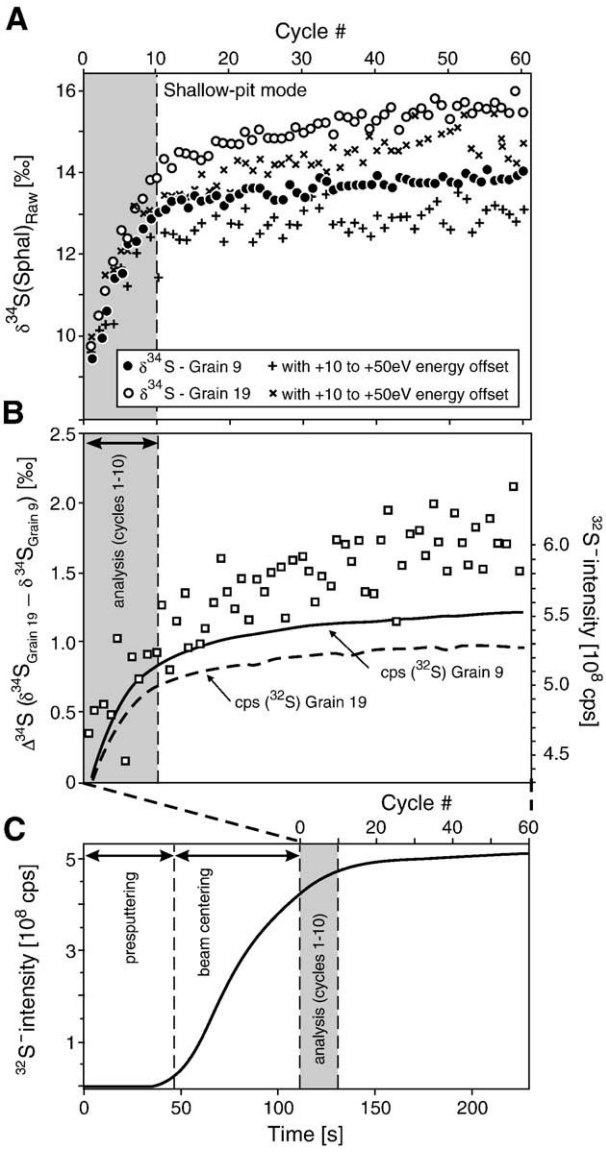

Fig. 7. A) Values of measured $\delta^{34}S_{Raw}$ are plotted for 60 two-second cycles of analysis on grains 9 and 19 of BT-4 sphalerite (compare with Fig. 5) in shallow pit mode. A presputtering time of 45 s and centering of the secondary ion image in the field aperture (~60 s) precedes the first analysis cycle. The difference in measured $\delta^{34}S$ between these two grains remains unchanged using an additional +10 eV energy offset. B) Solid and dashed lines show the change in secondary ion yield (^{32}S) of grains 9 and 19 during 60 two-second cycles, and white squares are the difference in measured $\delta^{34}S$ ($\delta^{34}S = \delta^{34}S(\text{grain 19}) - \delta^{34}S(\text{grain 9})$). In contrast to analyses in deep pit mode, where the difference in $\delta^{34}S$ between these grains remains constant at ~2.4‰ in the course of all analytical cycles (Fig. 5), measured $\delta^{34}S$ values of grains 9 and 19 in shallow pit mode are within 1‰ during the first ten analytical cycles and diverge further from each other after the secondary ion signal stabilizes. Thus, the best grain-to-grain precision is attained if the analysis is performed within the first ten cycles (grey bar). By following this analytical procedure, the difference in measured $\delta^{34}S$ between grain 9 and grain 19 was reduced from 2.4‰ in deep-pit mode to 0.2‰ in shallow pit mode (Supplementary data, Table 3). C) The optimum time of sputtering before the ten analytical cycles shown in B) was determined by a presputtering test. Changes in primary beam intensity affect the rate of increase in secondary ion yield and thus consistent technique is important.

characterized by nonzero values of $\Delta^{33}S$ in samples older than ~2.4 Ga. Sulfur isotope anomalies have been identified in pyrite, pyrrhotite, chalcopyrite, and galena from the Archean geologic record (cf. Seal, 2006; Philippot et al., 2007). MIF-S signatures in small samples have been previously analyzed by SIMS (e.g. Mojzsis et al., 2003; Whitehouse et al., 2005; Papineau et al., 2007). With respect to the findings of this study, it is important to emphasize that MIF signatures determined by SIMS are likely unaffected by crystal

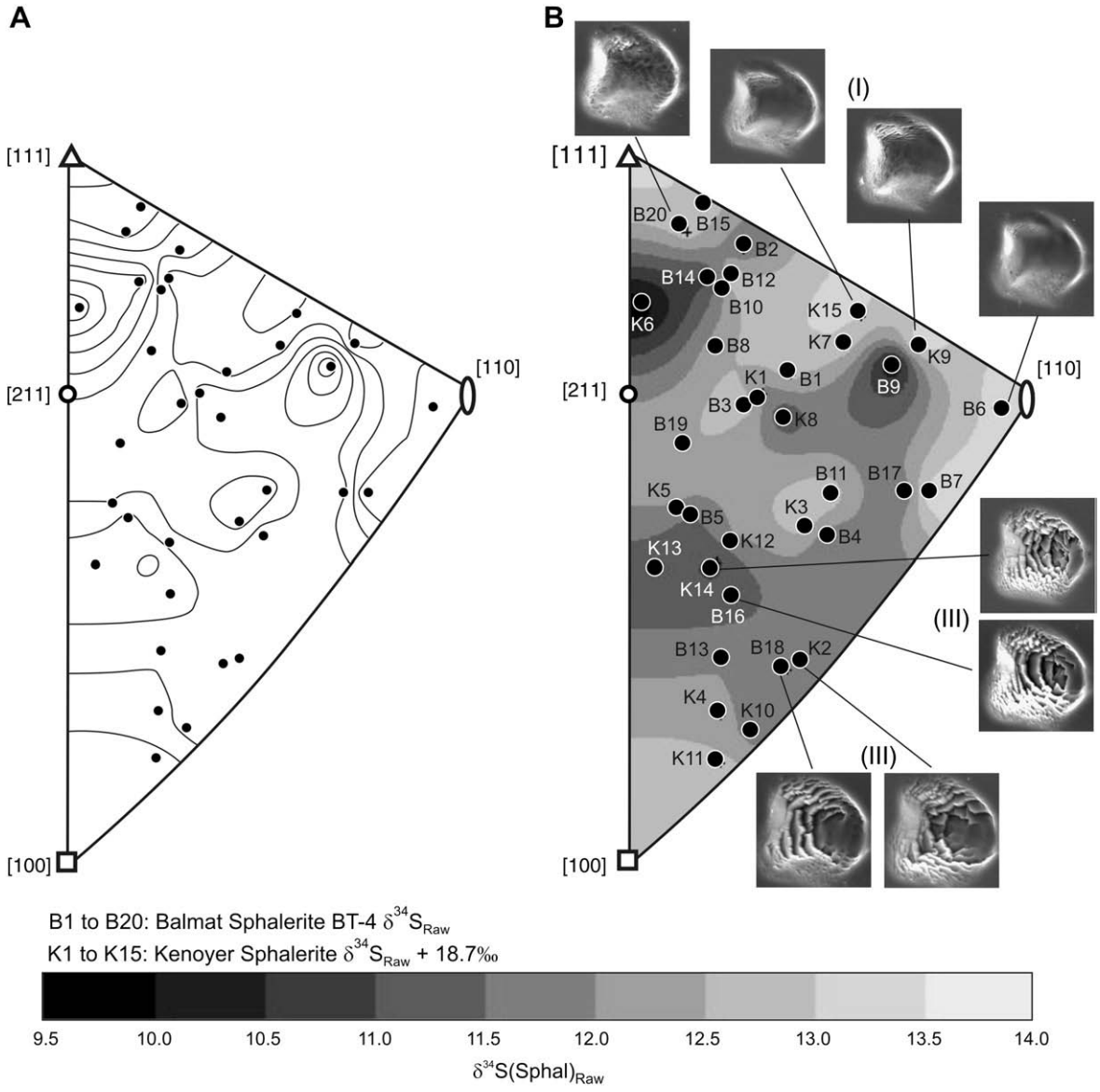

Fig. 8. (A) The standard triangle for a stereographic projection of a cubic symmetry mineral is shown contoured for $\delta^{34}S(Sphal)_{Raw}$ of Balmat Sphalerite BT-4 and Kenoyer Sphalerite analyzed in deep-pit mode. The directions [110], [100], and [111] define the standard triangle for cubic crystal structures. The stereographic projection of the Cs^+ beam direction is plotted for individual sphalerite grains (crosses) and 0.5‰ contours are derived from block kriging. (B) Shaded contour map. Balmat BT-4 sphalerite grains are labeled B1 to B20, and sphalerite grains from the Kenoyer Mine are labeled K1 to K15. Highest $\delta^{34}S(Sphal)_{Raw}$ values are measured when the Cs^+ beam is parallel to the set of directions <*uuw*>, from [111] to [110], preferred directions for channeling and focusing in diamond-centered cubic crystals. (I) SIMS analysis pits parallel to the set of directions <*uuw*> feature smooth crater walls. (II and III) Individual grains of Balmat Sphalerite BT-4 and Kenoyer Sphalerite, which were analyzed in similar orientation relative to the Cs^+ beam, show identical pit microstructures.

orientation effects, as the normal processes causing analytical bias (instrumental mass fractionation) are mass dependent (Heck et al., 2010).

5.2. Sulfur-isotope thermometry by SIMS

The measurement of $\delta^{34}S$ values in sub-20 µm grains of pyrite and sphalerite in Archean cherts (Fig. 11) with an analytical precision of ±0.2‰ in pyrite and ±0.8‰ (2SD) in sphalerite has shown that the analytical technique developed in this study is for *in situ* sulfur isotope thermometry in appropriate samples. Utilizing *in situ* SIMS analysis for isotope thermometry is a promising approach due to the small spatial resolution of SIMS measurements and the possibility to analyze small or zoned mineral grains that would be impossible otherwise.

Mississippi Valley-type Pb–Zn deposits provide an example of the precision and accuracy that are possible. Temperatures of formation are typically estimated at 100 °C–150 °C from independent means such as fluid inclusions. Sulfur isotope measurements by SIMS with a precision of ±0.3‰ for $\delta^{34}S$ ($\Delta^{34}S$(pyrite–chalcopyrite) ±0.42‰) in the mineral pair pyrite–chalcopyrite allow temperature estimates with an analytical uncertainty of ±25 °C (Kajiwara and Krouse, 1971) for spots 10 µm in diameter. This is a significant improvement from previous SIMS studies that performed measurements of $\delta^{34}S$ in chalcopyrite, pyrrhotite, and pyrite with ~25 µm spot size and an analytical precision of ±0.7‰. Further, the precision of ±0.3‰ within single crystals of sphalerite can be used to measure zoning profiles in grains that have been analyzed by conventional approaches. Thus, homogeneity in single grains of sphalerite could be verified and anomalous temperatures can be evaluated in published studies.

5.3. Implications for previous studies

The findings of this study reveal that variations in the sulfur isotope composition in sphalerite measured by ion microprobe

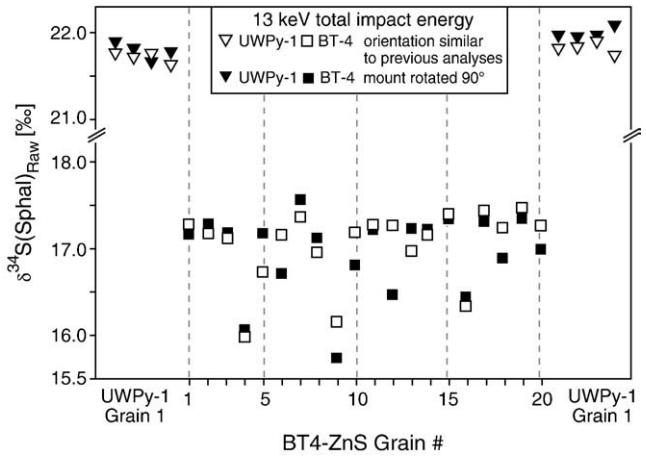

Fig. 9. Values of $\delta^{34}S_{Raw}$ are plotted for 20 grains of BT-4 sphalerite and the bracketing UWPy-1 pyrite standard, analyzed at 13 keV total impact energy in two different orientations in the grain mount with respect to the incident Cs^+ primary beam. White symbols indicate the orientation that was used for all previous measurements in this study, and black symbols show measured $\delta^{34}S_{RAW}$ values of the same set of grains after the sample mount was rotated by 90° (compare with Fig. 6 for the reproducibility of multiple measurements within a single grain without sample rotation).

(Riciputi et al., 1998; Bawden et al., 2003; Peevler et al., 2003) can be — to some extent — attributed to crystal orientation effects, which are superimposed on the natural variation in the sample. The amplitude of crystal orientation effects varies depending on instrumentation and the analytical parameters and has to be determined for every laboratory individually. For example, for measurements performed in routine analytical conditions at WiscSIMS (deep-pit mode, 20 keV), crystal orientation effects in sphalerite lead to a grain-to-grain precision of ±1.7‰ (2SD) that could be mistaken as natural sample variability. It is likely that this effect is greater for SIMS instruments using stronger beams and longer analysis times, thus forming deeper analysis pits. In order to differentiate between crystal orientation effects on $\delta^{34}S$ and natural sample variability, it is imperative to perform measurements on multiple, randomly oriented grains of sphalerite standard and to evaluate the impact of crystal orientation effects on instrumental bias with the current analytical conditions.

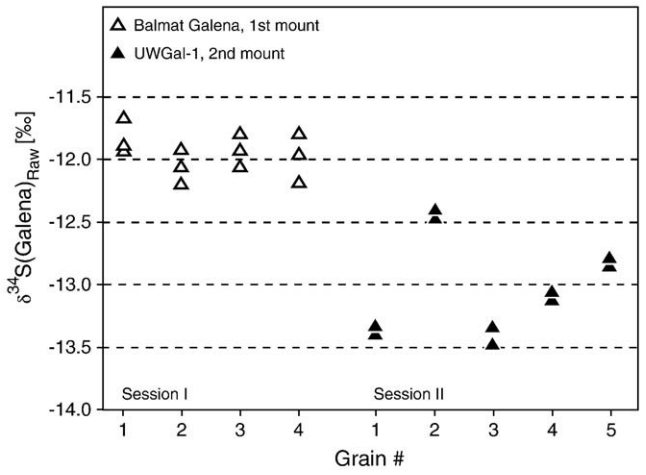

Fig. 10. Values of $\delta^{34}S(Galena)_{Raw}$ for galena from two samples from the Balmat mine, analyzed during different analytical sessions in deep pit mode. As a result of the perfect cleavage along {100}, crushed chips of galena are typically cube-shaped and have the potential to be preferentially oriented. In the first mount (Session I), individual grains of Balmat galena were oriented with [100] parallel to normal, resulting in a grain-to-grain precision of 0.3‰ (2SD, $n=12$). In the second mount, (Session II), individual grains of UWGal-1 (rock sample BT-100) were randomly oriented, and the grain-to-grain precision is worse at ±0.8‰ (2SD, $n=10$).

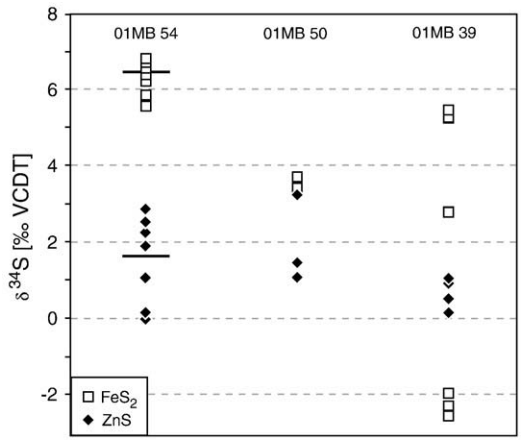

Fig. 11. Values of $\delta^{34}S$ for pyrite and coexisting sphalerite (15–70 μm diameter grains) in ~3.5 Ga cherts sampled at the North Pole Area, Old Exploration Camp (01MB 54 and 01MB 50) and the Trendall Locality (01MB 39), Pilbara Craton, Western Australia. Black horizontal bars indicate the average $\delta^{34}S$ values for pyrite and sphalerite in sample 01MB 54. The average Δ(pyrite–sphalerite) value of 4.6‰ in this sample is outside the range of equilibrium isotopic fractionation factors determined for this sulfide pair (Δ(pyrite–sphalerite) <4‰, Kajiwara and Krouse, 1971). Thus pyrite and sphalerite are not in isotopic equilibrium and these cherts are unsuitable for sulfur isotope thermometry.

6. Conclusion

In situ sulfur isotope measurements by SIMS were performed with a grain-to-grain precision of ±0.3‰ in chalcopyrite, galena, and pyrrhotite, and ±0.2‰ in pyrite (2SD). This excellent precision was achieved using a Gaussian focused Cs^+ beam with 10 μm spot size, creating SIMS analysis pits that are a few μm deep. A similar precision is attained for $\delta^{34}S$ measurements within single crystals of sphalerite. However, the best grain-to-grain precision achieved for sphalerite in this analytical condition was ±1.7‰ (2SD). Thus, if only a single grain of sphalerite is analyzed by SIMS, the analyses of samples would seem precise at ±0.3‰, but could be inaccurate by up to 3‰ if the standard grain has a different orientation. Measured $\delta^{34}S$ values in sphalerite correlate to rippled textures seen in the bottoms of analysis pits, whereas pits formed in other sulfide minerals are smooth. This ripple formation in sphalerite is associated with a higher secondary ion yield and lower $\delta^{34}S(Sphal)_{Raw}$ values. Measurements of crystal orientation by EBSD reveal that high $\delta^{34}S(Sphal)_{Raw}$ values (low secondary ion yield) are measured when the incident Cs^+ beam is parallel the set of directions <*uuw*> from [111] to [110], preferred directions of channeling and focusing in diamond-centered cubic crystals. The precision of $\delta^{34}S$ measurements in sphalerite can be improved by either reducing the depth of the analysis pits using a Köhler illuminated beam, or by lowering the total impact energy of the primary ions from 20 keV to 13 keV. In both approaches, the grain-to-grain precision of $\delta^{34}S$ measurements in sphalerite improved from ±1.7‰ to ±0.6‰. The development of this analytical technique for high precision sulfur isotope measurements in sulfides by SIMS will be important in future studies such as *in situ* S-isotope thermometry.

Acknowledgments

The authors thank Brian Hess for careful sample preparation; Taka Ushikubo for fruitful discussions; Jim Kern for technical support; Virginia Toy for assistance with EBSD analysis and software handling; Doug Crowe for providing samples, and Arthur Hickman, Aaron Cavosie, and David Valley for assistance in collection of Pilbara cherts. Ian Williams and an anonymous reviewer made helpful comments that improved the manuscript. We thank Roberta Rudnick for editorial handling. This study was funded by The NASA Astrobiology Institute,

NSF-EAR (0509639, 0838058), and DOE (93ER14389). WiscSIMS is partly supported by NSF-EAR (0319230, 0516725, 0744079).

Appendix A. Supplementary data

Supplementary data associated with this article can be found, in the online version, at doi:10.1016/j.chemgeo.2010.05.015.

References

Armstrong, J.T., 1988. Quantitative analysis of silicates and oxide minerals: comparison of Monte-Carlo, ZAF and Phi-Rho-Z procedures. In: Newbury, D.E. (Ed.), Proc. Microbeam Analysis Society. San Francisco Press, San Francisco, pp. 239–246.

Bawden, T.M., Einaudi, M.T., Bostick, B.C., Meibom, A.M., Wooden, J., Norby, J.W., Orobona, M.J.T., Chamberlain, C.P., 2003. Extreme ^{34}S depletions in ZnS at the Mike gold deposit, Carlin Trend, Nevada: evidence for bacteriogenic supergene sphalerite. Geology 31, 913–916.

Brasier, M., McLoughlin, N., Green, O., Wacey, D., 2006. A fresh look at the fossil evidence for early Archaean cellular life. Philos. Trans. R. Soc. London, Ser. B: Biol. Sci. 361, 887–902.

CAMECA, 2004. IMS 1270/80 Ion Optics User Guide. 510 pp.

Crowe, D.E., Valley, J.W., Baker, K.L., 1990. Micro-analysis of sulfur-isotope ratios and zonation by laser microprobe. Geochim. Cosmochim. Acta 54, 2075–2092.

Crowe, D.E., Vaughan, R.G., 1996. Characterization and use of isotopically homogeneous standards for *in situ* laser microprobe analysis of $^{34}S/^{32}S$ ratios. Am. Mineral. 81, 187–193.

Ding, T., Valkiers, S., Kipphardt, H., DeBièvre, P., Taylor, P.D.P., Gonfiantini, R., Krouse, R., 2001. Calibrated sulfur isotope abundance ratios of three IAEA sulfur isotope reference materials and V-CDT with a reassessment of the atomic weight of sulfur. Geochim. Cosmochim. Acta 65, 2433–2437.

Duncan, S., Smith, R., Sykes, D.E., Walls, J.M., 1983. Summary abstract: surface topography of electronic materials following oxygen and cesium ion bombardment. J. Vac. Sci. Technol., A 1, 621.

Eiler, J.M., Graham, C.M., Valley, J.W., 1997. SIMS analysis of oxygen isotopes: matrix effects in complex minerals and glasses. Chem. Geol. 138, 221–244.

Eldridge, C.S., Compston, W., Williams, I.S., Walshe, J.L., Both, R.A., 1987. *In situ* microanalysis for $^{34}S/^{32}S$ ratios using the ion microprobe SHRIMP. Int. J. Mass Spectrom. Ion Processes 76, 65–83.

Fares, B., Gautier, B., Baboux, N., Prudon, G., Hollinger, P., Dupuy, J.C., 2004. Influence of surface orientation on the formation of sputtering-induced ripple topography in silicon. Appl. Surf. Sci. 231–232, 678–683.

Farquhar, J., Bao, H., Thiemens, M., 2000. Atmospheric influence of Earth's earliest sulfur cycle. Science 289, 756–758.

Fayek, M., 2009. Hydrogen, carbon, nitrogen and sulfur isotope microanalysis by Secondary Ion Mass Spectrometry. In: Fayek, M. (Ed.), MAC Short Course: Secondary Ion Mass Spectrometry in the Earth Sciences, pp. 65–83.

Galley, A.G., Bailes, A.H., Kitzler, G., 1993. Geological setting and hydrothermal evolution of the Chisel Lake and North Chisel Zn–Pb–Cu–Ag–Au massive sulfide deposits, Snow Lake, Manitoba. Explor. Min. Geol. 2, 271–295.

Galouchko, V., 2008. 3DField Pro Version 2.0.2. http://3dfmaps.com.

Giesemann, A., Jäger, H.-J., Norman, A.L., Krouse, H.R., Brand, W.A., 1994. On-line sulfur-isotope determination using an elemental analyzer coupled to a mass spectrometer. Anal. Chem. 66, 2816–2819.

Gnaser, H., 2007. Energy and angular distributions of sputtered species. Sputtering by Particle Bombardment. : Topics in Applied Physics. Springer-Verlag, New York, pp. 231–328.

Graham, C.M., Valley, J.W., 1992. Sulphur isotope analysis of pyrites. Chem. Geol. 101, 169–172.

Heck, P.R., Ushikubo, T., Schmitz, B., Kita, N.T., Spicuzza, M.J., Valley, J.W., 2010. A single asteroidal source for extraterrestrial Ordovician chromite grains from Sweden and China: High-precision oxygen three-isotope SIMS analysis. Geochim. Cosmochim. Acta 74, 497–509.

Hervig, R.L., 2002. Anomalous fractionation of sulfur isotopes during sputtering. Rapid Commun. Mass Spectrom. 16, 1774–1778.

Hervig, R.L., Williams, P., Thomas, R.M., Schauer, S.N., Steele, I.M., 1992. Microanalysis of oxygen isotopes in insulators by secondary ion mass spectrometry. Int. J. Mass Spectrom. 120, 45–63.

Huberty, J.M., Kita, N.T., Kozdon, R., Heck, P.R., Fournelle, J.H., Spicuzza, M.J., Xu, H., Valley, J.W., in press. Crystal orientation effects in $\delta^{18}O$ for magnetite and hematite by SIMS. Chem. Geol.

Hut, G., 1987. Consultants' Group Meeting on Stable Isotope Reference Samples for Geochemical and Hydrological Investigations. International Atomic Energy Agency, Vienna, Austria, p. 43.

Kajiwara, Y., Krouse, H.R., 1971. Sulfur isotopic partitioning in metallic sulfide system. Can. J. Earth Sci. 8, 236–238.

Kaminsky, M., 1965. Atomic and ionic impact phenomena on metal surfaces. Struktur und Eigenschaften der Materie in Einzeldarstellungen., xii. Academic Press, New York. 402 pp.

Kita, N.T., Ushikubo, T., Fu, B., Valley, J.W., 2009. High precision SIMS oxygen isotope analysis and the effect of sample topography. Chem. Geol. 264, 43–57.

Lewis, G.W., Nobes, M.J., Carter, G., Whitton, J.L., 1980. The mechanisms of etch pit and ripple structure formation on ion bombarded Si and other amorphous solids. Nucl. Instrum. Methods 170, 363–369.

Lyon, I.C., Saxton, J.M., Cornah, S.J., 1998. Isotopic fractionation during secondary ionization mass spectrometry: crystallographic orientation effects in magnetite. Int. J. Mass Spectrom. Ion Processes 172, 115–122.

Malherbe, J.B., 2003. Bombardment-induced ripple topography on GaAs and InP. Nucl. Instrum. Methods Phys. Res., Sect. B 212, 258–263.

McKibben, M.A., Riciputi, L.R., 1998. Sulfur isotopes by ion microprobe. In: McKibben, M.A., Schanks, W.C.I., Ridley, W.I. (Eds.), Applications of Microanalytical Techniques to Understanding Mineralizing Processes: Society of Economic Geologists Reviews in Economic Geology, 7, pp. 121–139.

Mojzsis, S.J., Coath, C.D., Greenwood, J.P., McKeegan, K.D., Harrison, T.M., 2003. Mass-independent isotope effects in Archean (2.5 to 3.8 Ga) sedimentary sulfides determined by ion microprobe analysis. Geochim. Cosmochim. Acta 67 (9), 1635–1658.

Papineau, D., Mojzsis, S.J., Schmidt, A.K., 2007. Multiple sulfur isotopes from Paleoproterozoic Huronian interglacial sediments and the rise of atmospheric oxygen. Earth Planet. Sci. Lett. 255, 188–212.

Peevler, J., Fayek, M., Misra, K.C., Riciputi, L.R., 2003. Sulfur microanalysis of sphalerite by SIMS: constrains on the genesis of Mississippi valley-type mineralization, from the Mascot-Jefferson City district, East Tennessee. J. Geochem. Explor. 80, 277–296.

Philippot, P., Zuilen, M.V., Lepot, K., Thomazo, C., Farquhar, J., Van Kranendonk, M.J., 2007. Early Archaean microorganisms preferred elemental sulfur, not sulfate. Science 317, 1534–1537.

Pimminger, A., Grasserbauer, M., Schroll, E., Cerny, I., 1984. Microanalysis in galena by Secondary Ion Mass Spectrometry for determination of sulfur isotopes. Anal. Chem. 56 (3), 407–411.

Riciputi, L.R., Paterson, B.A., 1994. High spatial-resolution measurements of O isotope ratios in silicates and carbonates by ion microprobe. Am. Mineral. 79, 1227–1230.

Riciputi, L.R., Paterson, B.A., Ripperdan, R.L., 1998. Measurement of light stable isotope ratios by SIMS: matrix effects for oxygen, carbon and sulfur isotopes in minerals. Int. J. Mass Spectrom. 178, 81–112.

Röller, K., Trepmann, C., 2008. Stereo32 Version 1.01. http://www.ruhr-uni-bochum.de/hardrock/downloads.htm2008.

Schopf, J.W., Kudryavtsev, A.B., Agresti, D.G., Wdowiak, T.J., Czaja, A.D., 2002. Laser-Raman imagery of Earth's earliest fossils. Nature 416, 73–76.

Seal, R.R., 2006. Sulfur isotope geochemistry of sulfide minerals. Rev. Mineral. Geochem. 61, 633–677.

Stevie, F.A., Kahora, P.M., Simons, D.S., Chi, P., 1988. Secondary ion yield changes in Si and GaAs due to topography changes during O_2^+ or Cs^+ ion bombardment. J. Vac. Sci. Technol., A (1), 76–80.

Thode, H.G., MacNamara, J., Collins, C.B., 1949. Natural variations in the isotopic content of sulfur and their significance. Can. J. Res. 27B, 361–373.

Valley, J.W., Graham, C.M., 1991. Ion microprobe analysis of oxygen isotope ratios in metamorphic magnetite-diffusion reequilibration and implications for thermal history. Contrib. Mineral. Petrol. 109, 38–52.

Valley, J.W., Graham, C.M., 1996. Ion microprobe analysis of oxygen isotope ratios in quartz from Skye Granite: healed micro-cracks, fluid flow, and hydrothermal exchange. Contrib. Mineral. Petrol. 5, 158–173.

Valley, J.W., Graham, C.M., Harte, B., Kinny, P., Eiler, J.M., 1998. Ion microprobe analysis of oxygen, carbon, and hydrogen isotope ratios. In: McKibben, M.A. (Ed.), Soc. Econ. Geol. Rev. in Econ. Geol. , pp. 73–98.

Valley, J.W., Kita, N.T., 2009. *In situ* oxygen isotope geochemistry by ion microprobe. In: Fayek, M. (Ed.), MAC Short Course: Secondary Ion Mass Spectrometry in the Earth Sciences, pp. 16–63.

Whitehouse, M.J., Kamber, B.S., Fedo, C.M., Lepland, A., 2005. Integrated Pb- and S-isotope investigation of sulphide minerals from the early Archean of Southwest Greenland. Chem. Geol. 222, 112–131.